# RESCUe

## Reliable TT&C during superior solar conjunctions

Executive Summary

PREPARED BY RESCUE TEAM

**ISSUE** : 1
**REVISION** : 1
**DATE** : 6/9/2017



## TABLE OF CONTENTS

## CHANGE LOG

| ISSUE | ISSUE/REVISION | REASON | DATE |
|---|---|---|---|
| 1 | 1.0 | FIRST ISSUE OF THE DOCUMENT | 14/3/2017 |
| 1 | 1.1 | AFTER IMPLEMENTATION OF COMMENTS BY ESA | 8/6/2017 |

## LIST OF ACRONYMS

| ACRONYM | DESCRIPTION | ACRONYM | DESCRIPTION |
|---|---|---|---|
| ADC | ANALOG TO DIGITAL CONVERTER | LDPC | LOW-DENSITY PARITY-CHECK |
| AM | AMPLITUDE MODULATION | LGA | LOW GAIN ANTENNA |
| ASIC | APPLICATION SPECIFIC INTEGRATED CIRCUIT | LRL | LOW RATE LINK |
| AWGN | ADDITIVE WHITE GAUSSIAN NOISE | LUT | LOOK UP TABLE |
| BB | BASEBAND | MEX | MARS EXPRESS |
| BCH | BOSE CHAUDHURI HOCQUENGHEM | MRL | MEDIUM RATE LINK |
| BEC | BINARY ERASURE CHANNEL | MRB | MOST RELIABLE BASIS |
| BER | BIT ERROR RATE | NMS | NORMALIZED MIN SUM |
| BPSK | BINARY PHASE SHIFT KEYING | NRZ | NON RETURN TO ZERO |
| CC | CONVOLUTIONAL CODE | OBC | ON-BOARD COMPUTER |
| CCSDS | CONSULTATIVE COMMITTEE FOR SPACE DATA SYSTEMS | PCB | PRINTED CIRCUIT BOARD |
| CER | CODEWORD ERROR RATE | PCM | PULSE CODE MODULATION |
| CLTU | COMMUNICATIONS LINK TRANSMISSION UNITS | PCTC | PARALLEL CONCATENATED TURBO CODE |
| CNIT | CONSORZIO NAZIONALE INTERUNIVERSITARIO PER LE TELECOMUNICAZIONI | PDF | PROBABILITY DENSITY FUNCTION |
| DDR | DOUBLE DATA RATE | PLL | PHASE LOCKED LOOP |
| DDS | DIRECT DIGITAL SYNTHESIS | PM | PHASE MODULATION |
| DPRAM | DUAL-PORTED RANDOM ACCESS MEMORIES | RAM | RANDOM ACCESS MEMORY |
| DPSK | DIFFERENTIAL PHASE SHIFT KEYING | ROM | ROUGH ORDER OF MAGNITUDE |
| DSP | DIGITAL SIGNAL PROCESSING | RS | REED-SOLOMON |
| DST | DEEP SPACE TRANSPONDER | RSCC | REED-SOLOMON CONVOLUTIONAL CODE |
| ELRL | EXTREMELY LOW RATE LINK | SAW | SURFACE ACOUSTIC WAVE |
| ESA | EUROPEAN SPACE AGENCY | SEP | SUN-EARTH-PROBE |

| | | | |
|---|---|---|---|
| FP | FADING PERIOD | SNR | SIGNAL-TO-NOISE RATIO |
| FPGA | FIELD PROGRAMMABLE GATE ARRAY | SSB | SINGLE SIDE BAND |
| FSK | FREQUENCY SHIFT KEYING | S/W | SOFTWARE |
| GMSK | GAUSSIAN MINIMUM SHIFT KEYING | TAS-I | THALES ALENIA SPACE ITALIA |
| HPA | HIGH POWER AMPLIFIER | TC | TELECOMMAND |
| HRL | HIGH RATE LINK | TM | TELEMETRY |
| H/W | HARDWARE | TT&C | TRACKING, TELEMETRY AND COMMAND |
| IBO | INPUT BACK-OFF | TWTA | TRAVELLING WAVE TUBE AMPLIFIER |
| IF | INTERMEDIATE FREQUENCY | | |

## APPLICABLE DOCUMENTS

| DOC ID | REFERENCE |
|---|---|
| [AD 1] | 207, REV. A, '34-M AND 70-M TELEMETRY RECEPTION', DSMS TELECOMMUNICATIONS LINK DESIGN HANDBOOK, 810-005, REV. E, JUNE 13, 2003 |
| [AD 2] | FLOYD M. GARDNER, "PHASELOCK TECHNIQUES", WILEY, 1979 |
| [AD 3] | CCSDS, "SHORT BLOCK LENGTH LDPC CODES FOR TC SYNCHRONIZATION AND CHANNEL CODING," APR. 2015, ORANGE BOOK, CCSDS 231.1-O-1 |
| [AD 4] | CCSDS, "TC SYNCHRONIZATION AND CHANNEL CODING – SHORT BLOCKLENGTH LDPC CODES," OCT. 2016, GREEN BOOK, 230.1-G-X |
| [AD 5] | CCSDS, "TM SYNCHRONIZATION AND CHANNEL CODING," AUG. 2011, BLUE BOOK, CCSDS 131.-B-2 |
| [AD 6] | LDPC DECODER ARCHITECTURAL DESIGN, REF: TN-LDPC-DEC-ADD, ISSUE 2.1, 2016-04-04 |

## REFERENCE DOCUMENTS

| DOC ID | REFERENCE |
|---|---|
| [RD 1] | D. MORABITO, 'SOLAR CORONA AMPLITUDE SCINTILLATION MODELING AND COMPARISON TO MEASUREMENTS AT X-BAND AND KA-BAND', TDA PROGRESS REPORT 42-153, MAY 15, 2003 |
| [RD 2] | CCSDS, "TM SYNCHRONIZATION AND CHANNEL CODING - SUMMARY OF CONCEPT AND RATIONALE," NOV. 2012, GREEN BOOK, CCSDS 130.1-G-2. |
| [RD 3] | CCSDS, "TM SYNCHRONIZATION AND CHANNEL CODING - SUMMARY OF CONCEPT AND RATIONALE," NOV. 2012, GREEN BOOK, CCSDS 230.1-G-2. |
| [RD 4] | P. MAGUIRE, M. WESTCOTT, R. ABELLO, "DEVELOPMENT OF A LDPC CODEC FOR THE TTCP," TT&C2016, ESA-ESTEC |

## 1. STUDY CONTEXT

The radio link between deep space probes and Ground Stations is degraded, and in some cases severely impaired up to interruption, during superior solar conjunctions by the effects of the solar corona the signal crosses. The solar corona and the interplanetary medium are turbulent media characterized by a refractive index varying both in time and space. Although the corrections to the vacuum refracting index are small at microwave frequencies, the effects are quite significant when the plasma density is sufficiently large, as in the case of the solar corona. The main effects on the radio link, relevant to this study, are the amplitude and phase scintillations.

With reference to Figure 1-1, after passing through the screen, the plane wave front suffers a distortion due to the different path delays along the slab. After emerging from the screen, the electric field suffers a phase rotation different at each point, depending on the local refractive index. The phase fluctuations are called phase scintillation. Immediately after emerging from the screen, the electric field phase fluctuates, but the amplitude is constant, as no absorption occurred. However, at large distances from the screen, the diffraction due to the individual scatterers produce randomly constructive or destructive interferences (Figure 1-1). The electric field fluctuations in time at a given location are identified as amplitude scintillation. The spectrum of density fluctuations in the solar wind is well approximated by a Kolmogorov spectrum, whose power law dependence on the wavenumber $k$ is a consequence of the non-linear interaction among vortices (the $v \cdot \nabla v$ term in Navier-Stokes equation, where $v$ is the velocity).

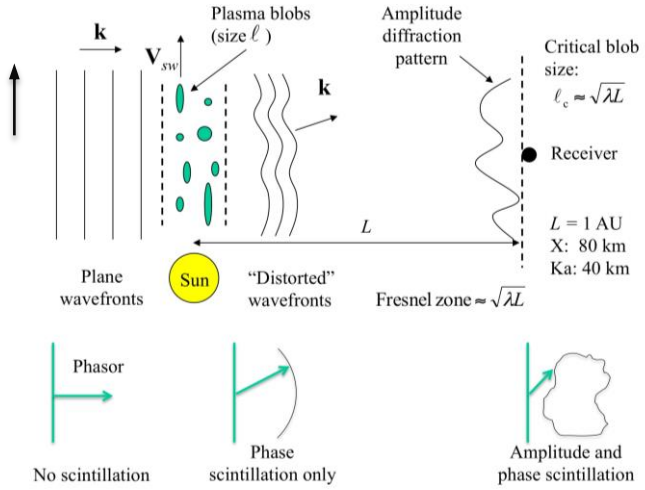


Figure 1-1: schematic diagram of phase and amplitude scintillation in the thin screen approximation.

## 2. STUDY GOAL AND APPROACH

The study aims at investigating technical solutions to design a reliable TT&C system during superior solar conjunctions, to mitigate the detrimental effects of phase and amplitude scintillation, which limit the maneuvers under 5 deg of Sun-Earth-Probe (SEP) angle.

After the analysis of data acquired during superior solar conjunctions of Mars Express (MEX) in 2013-2015 and Cassini in 2001-2002, that allowed deriving a mathematical model to be used in the simulations, the current ESA TT&C system has been evaluated, in terms of link performance. Then, technical solutions in several domains (modulation, coding, and system diversity) have been proposed and evaluated using software tools, a baseband and an end-to-end simulator. Finally, the implementation steps for the identified solutions and the roadmap for the next 10 years have been addressed.

The team is composed of Arpsoft as Prime Contractor, Thales Alenia Space Italia (TAS-I) and Consorzio Nazionale Interuniversitario per le Telecomunicazioni (CNIT) as sub-contractors.

## 3. CASSINI AND MARS EXPRESS DATA ANALYSIS

The evaluation of the link performance has been carried out with numerical simulations, both baseband and end-to-end. In any case, a mathematical model to use in the software tools has been derived from the analysis of open loop data acquired during superior solar conjunctions of Mars Express in 2013-2015 and Cassini in 2001-2002. Such data analysis allowed the characterization of the phase and amplitude scintillations from a spectral and probability density function (PDF) perspectives.

Regarding the phase scintillation, Cassini open loop data stream was fed into a digital phase locked loop (PLL), and the received sky frequencies were reconstructed. The sky frequencies were then fitted with a 6 parameters fit, in order to absorb the Doppler shift caused by the spacecraft dynamics. For Mars Express, instead, the Doppler residuals were provided directly by ESA, as the 6 parameters fit was not accurate enough for an orbiting spacecraft.

The power spectra of the frequency residuals were investigated for different bands (X, Ka) and different SEP angles, in order to determine the range of applicability of the Kolmogorov turbulence theory to phase scintillation characterization. The so-called Kolmogorov spectrum exhibits a $-11/3$ power law in the power spectrum of the density fluctuations. Following this theory, the power law of the frequency residuals shall be $-2/3$. Figure 3-1 shows that the computed index of the power law of the frequency residuals is the expected one. Also, Figure 3-1 shows a quite large variability in the power law index of X band data. This is due to the larger sensitivity of the X band to the plasma scintillation. In Ka band, that is less sensitive to the scintillation, the power law index matches well the one predicted by the Kolmogorov theory. Such value has been taken as input for the simulation of the phase contribution to the signal.

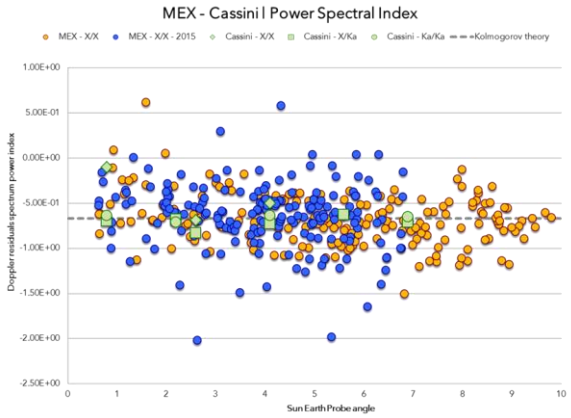


Figure 3-1: power spectral index of Doppler residuals vs SEP angle and comparison to Kolmogorov predicted value.

Also, from the power spectrum it is possible to extract the power content of the plasma noise to be applied in the simulator. From the fit of the spectrum in the range of frequencies where the plasma is present, by using a power law having –2/3 as exponent, is possible to derive the power content of the plasma at 1 Hz frequency.

Regarding the amplitude scintillation, its modelling available in literature, confirmed with the data analysis, considers that the PDF of the signal amplitude can be well represented with a Rice distribution. The mean and variance of the Rice distribution depend on the scintillation index $m$, defined as the ratio between the standard deviation and the mean value of signal power. The scintillation index is related to the strength of the scattering. In scattering theory, the function $U$ can be used to model the strength of the wave fluctuations. $U$ is function of the propagating signal path and frequency, the "level" of the charged-particle density perturbations and the power-law index of the refractive index fluctuation spectrum $p$ [RD 1]. Integrating the $U$-Function is possible to retrieve the index scintillation $m$ as $\sqrt{U}$ for $0 < U < 1$ and 1 for $U \geq 1$.

The Rice distribution characterizes only the PDF of the amplitude fading, but not the evolution in time. For this reason, the data analysis was aimed also at defining the coherence time, defined as the time duration over which the channel response is invariant. Basically, the coherence time has been taken as parameter for the evolution in time of the fading amplitude. The coherence time has been computed from the amplitude spectrum. In this case, the bandwidth spanning from zero to the frequency at which the noise floor starts is the inverse of the coherence time. The same results can be attained from the autocorrelation of the amplitude, which, in turn, is related to its spectrum. The computation of the coherence time, for different scintillation index values, from the amplitude spectrum of Cassini and Mars Express data, for X and Ka band, is reported in Figure 3-2.

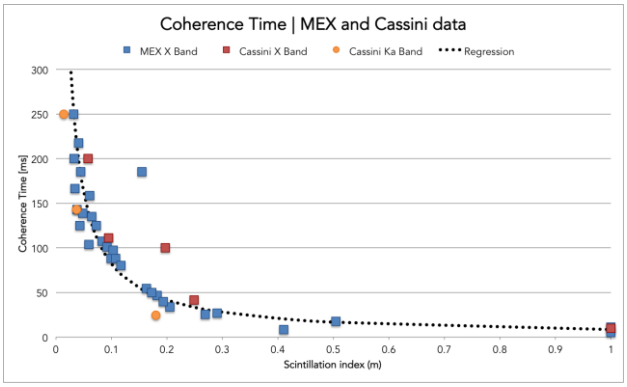


Figure 3-2: Mars Express and Cassini - coherence time vs scintillation index.

As expected [RD 1], the coherence time varies from a few ms at very low SEP angles to hundreds of ms at relatively large SEP angles.

## 4. CHARACTERIZATION OF PLL RESPONSE IN PRESENCE OF PLASMA SCINTILLATION

The characterization of the PLL has been a crucial point of the study. In fact, the analysis has allowed for the definition of the optimal setup, in terms of PLL bandwidth $B_L$, to track the carrier in presence of plasma scintillation. Moreover, the definition of the optimum PLL bandwidth drove the type of tests carried out. In fact, depending on the PLL bandwidth, it is possible to assume that the outcomes of the end-to-end tool are in full agreement with those attained using a baseband simulator.

### 4.1. OPTIMUM PLL BANDWIDTH AND EQUIVALENT LOOP SIGNAL TO NOISE RATIO

The PLL is subject to thermal noise and plasma scintillation. While the error variance of the former is proportional to the PLL bandwidth, for the latter the dependence is inverse. In fact, the data analysis has shown that the error variance due to plasma ${\sigma_{Pl}}^2$ can be expressed as:

$$ {\sigma_{Pl}}^2 = \frac{C_{band} C_{Loop}}{(\sin SEP)^{3.455} {B_L}^{1.55}} \qquad \text{Eq. 4-1} $$

being $C_{band}$ and $C_{Loop}$ two constants characteristic ([AD 1]), respectively, of the carrier band and the type of loop of the receiver. Minimizing the total error variance, with respect to $B_L$, results in the optimum PLL bandwidth $B_{OPT}$, and the equivalent loop SNR[1] associated:

[1] Defined as half the inverse of the error variance.

$$B_{OPT} = \sqrt[2.55]{\frac{1.55 C_{band} C_{loop}}{(\sin SEP)^{3.455}} \frac{P_c}{N_0 k_{th}(m)}} \qquad \text{Eq. 4-2}$$

$$k_{th} = \max(1 - 0.3942m + 4.9544m^2 - 9.4984m^3 + 6{,}5567m^4, 1)$$

$$SNR_{PLL} = \frac{1}{2\sigma_{PLL}^2} = \frac{P_c}{N_0 2B_{OPT} k_{th}(SEP) + 2P_c \frac{C_{band} C_{Loop}}{(\sin SEP)^{3.455} B_{OPT}{}^{1.55}}} \qquad \text{Eq. 4-3}$$

being $P_c/N_0$ the carrier power to noise density ratio and $k_{th}$ a degradation factor due to the amplitude scintillation.

The optimum bandwidth does not guarantee, per se, a proper carrier recovery. In fact, the end-to-end tests (confirmation of what reported in [AD 1]) have evidenced that the minimum equivalent loop SNR that provides a good carrier recovery is 7 dB. Thus, the equivalent loop SNR shall be computed in correspondence of the optimum bandwidth to verify it is above the threshold. Different values of $P_c/N_0$ and $B_L$ result in a region of operability of the bandwidth, in which the requirement of 7 dB is met.

Figure 4-1 shows the region of operability as a function of $P_c/N_0$ and double-sided PLL bandwidth for X and Ka band at 1 deg SEP. The red region identifies the non-operable bandwidths. The green region (dark + light) is the operability region for Ka-band, while the light green only region refers to X-band. Dashed lines mark the optimum bandwidths [dark green: Ka-band, light green: X-band].

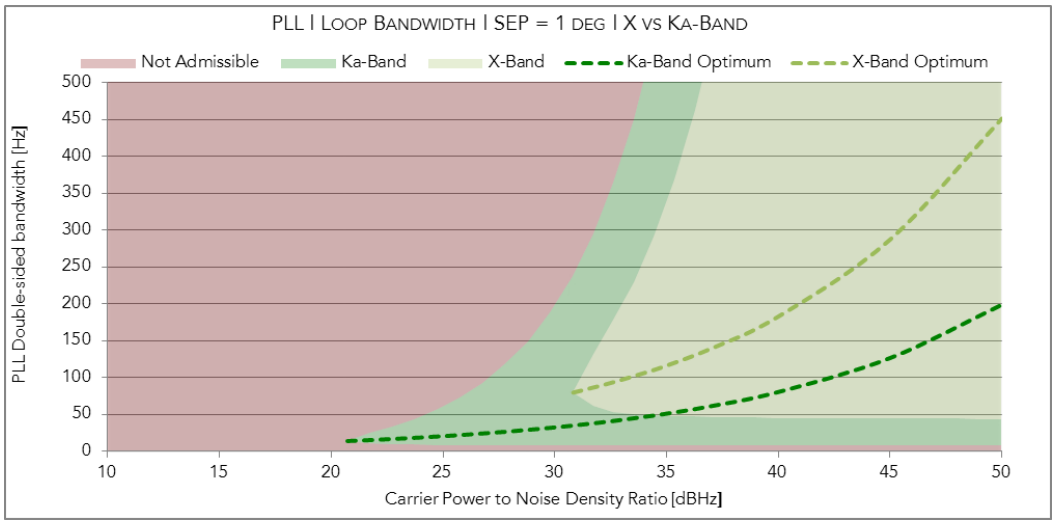


Figure 4-1: PCM/BPSK/PM - Operable PLL double-sided bandwidths at X- and Ka-band for different $P_c/N_0$ (SEP = 1 deg).

Results attained for PCM/BPSK/PM can be extrapolated for GMSK modulation. In particular, as the carrier recovery process is not de-coupled from the data noise, there is a squaring loss, dependent on the symbol energy to noise density ratio $E_s/N_0$, to take into account in the equivalent loop SNR. Such loss has to be accounted for in the computation of the equivalent SNR. In particular, having in mind that $P_c/N_0$ must be replaced by $P/N_0$, the optimum bandwidth can still be computed using Eq. 4-2, but the equivalent SNR computed with Eq. 4-3 has to be increased by an amount equal to the squaring loss (in negative sign).

Figure 4-1 has been produced for GMSK (Figure 4-2), assuming a symbol rate of 65.2 ksps.

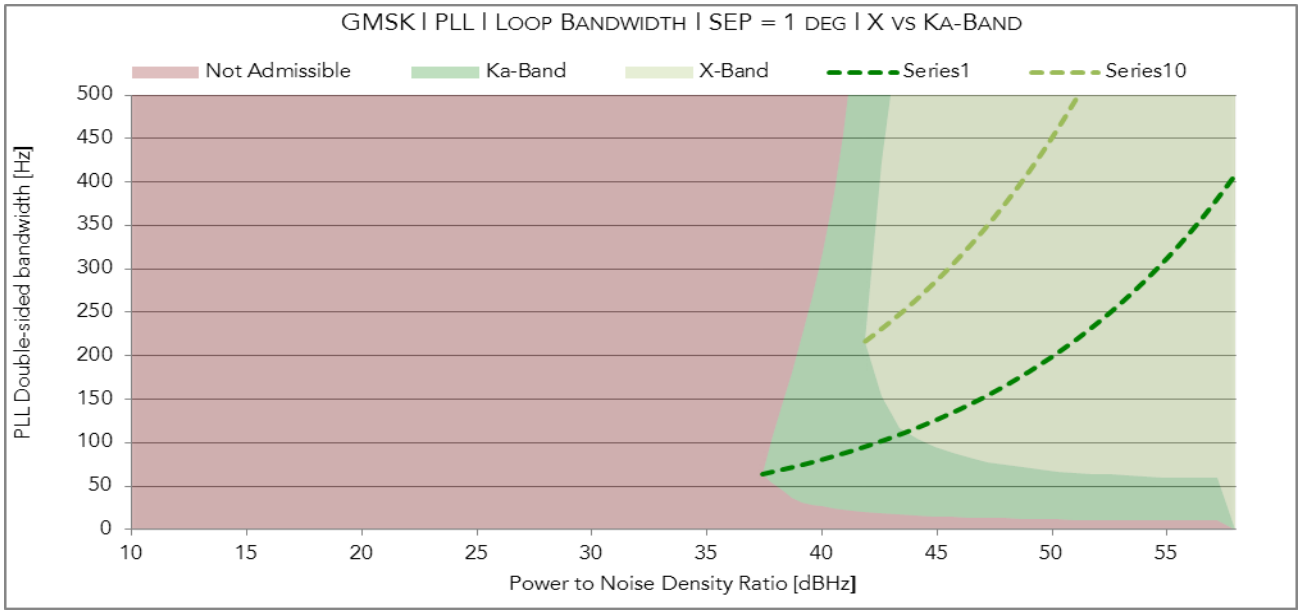


Figure 4-2: GMSK - Operable PLL double-sided bandwidths at X- and Ka-band for different $P_c/N_0$ (SEP = 1 deg).

## 5. PERFORMANCE OF CURRENT ESA TT&C ARCHITECTURE

A complete assessment of the current TT&C system performance, in terms of bit error rate/codeword error rate (BER/CER), has been carried out. The current deep space communications use, as standard, phase modulation schemes. Therefore, the modulation used for the tests has been set to PCM/BPSK/PM. As for the coding schemes used as standard in deep space missions, the techniques analyzed are:

- Bose Chaudhuri Hocquenghem (BCH) in telecommand (TC);
- Reed-Solomon + Convolutional Codes (RSCC) in telemetry (TM);
- Parallel Concatenated Turbo Codes (PCTC) in telemetry.

A detailed description of the structure, properties and performance of the various families of codes is reported in [RD 2] for TM links and in [RD 3] for TC links. The tests have been performed in two ways:

- Baseband tests: the PLL can be setup with a bandwidth such that the equivalent loop SNR is well above the limit of 7 dB. In this case, the removal of the phase scintillation can be considered complete (basically, the loss in the synchronization loops is null), and the performance degradation, due to amplitude scintillation on the signal, can be assessed with a baseband simulator, thus not simulating the recovery process.
- End-to-end tests: a few contingency scenarios are evaluated, where the $P_c/N_0$ and the SEP angle are such that the equivalent loop SNR is closer to the limit of 7 dB (and sometimes lower than that). The carrier recovery loop, as well as the remaining demodulation steps, must be simulated to properly assess the performances.

### 5.1. BASEBAND TESTS

Bypassing the synchronization loops, assuming to have used a PLL bandwidth that absorbs the phase contribution due to plasma, allows to reduce the computational time and to run a large number of tests on a variety of coding schemes that otherwise would not be possible with the end-to-end software.

Depending on the data rate $R_b$ and the coherence time $T_c$, four different operation regimes can be defined:

1. Extremely (or “Ergodic”) low rate links (ELRL): where the statistical averages over the encoded symbol fairly represent the average over all time;
2. Low rate links (LRL): where the channel varies during the transmission of an encoded symbol;

3. Medium rate links (MRL): where the channel does not vary during the transmission of an encoded symbol but varies during the transmission of a codeword;
4. High rate links (HRL): where the channel does not vary during the transmission of a codeword.

A large number of tests has been carried out in all the regimes, but, as most likely the link is confined in the MRL regime (as demonstrated in the technical notes of the study), the results are shown in MRL.

A parameter that is used in the simulations (and crucial to understand the results) is the *fading period FP*, which represents the amplitude fading period, expressed in encoded symbols for the sake of simplicity. The *FP* is basically the ratio between the coherence time and the symbol time. According to its definition, the value of *FP* must be specified for the LRL and the MRL scenarios. For the ELRL scenario it has no sense, while for the HRL scenario it is at least equal to the codeword length, as the channel remains constant for the duration of a codeword.

Table 5-1 to Table 5-3 show examples of performance of BCH (TC), RSCC and PCTC (TM) for different values of the scintillation index. In Table 5-1 and Table 5-2 the Additive White Gaussian Noise (AWGN) channel has been assumed as a reference.

| | *m = 0.2* | *m = 0.5* | *m = 0.9* |
|---|---|---|---|
| *FP* = 8 ENCODED SYMBOLS | 0.77 | 16.42 | 34.84 |
| *FP* = 32 ENCODED SYMBOLS | 1.04 | 17.03 | 35.48 |

Table 5-1: loss (in dB) at BER = 1E–5 (with respect to the AWGN channel), which is due to the presence of amplitude scintillation in the MRL scenario for BCH and two values of *FP*.

| *m* = 0.2 | *m* = 0.5 | *m* = 0.9 |
|---|---|---|
| 0.49 | 2.43 | 8.01 |

Table 5-2: loss (in dB) at CER = 1E–5 (with respect to the AWGN channel) which is due to the presence of amplitude scintillation in the MRL scenario for RSCC and *FP* = 150 encoded symbols.

| | *m* = 0.2 | *m* = 0.5 | *m* = 0.9 |
|---|---|---|---|
| PCTC(17848, 8920) | 1.50 | 5.48 | 13.47 |
| PCTC(35696, 8920) | 0.48 | 3.71 | 12.25 |
| PCTC(53544, 8920) | 0.25 | 2.78 | 11.13 |

Table 5-3: $E_b/N_0$ values (in dB) required to achieve CER = 1E–5 for the PCTC codes in the MRL scenario, assuming *FP* = 150 encoded symbols.

### 5.2. END-TO-END TESTS

The end-to-end tests have been performed to a) evaluate the link performance in contingency scenarios and b) demonstrate that, by choosing the optimum PLL bandwidth and/or a different data rate, the link can be made more reliable. As an example, Table 5-4 reports the nominal and optimized setup for a hypothetical scenario at Mars with a Low Gain Antenna (LGA). The nominal setup foresees a nominal $2B_L$ of 25 Hz, as the standard process in operations considers the plasma scintillation a loss in the available power. This results in an equivalent loop SNR of 3.18 dB, making the case unsuccessful. Given the results on the optimum PLL, it can be seen that enlarging the bandwidth allows to get an equivalent loop SNR of 11.35 dBHz, and the end-to-end run has demonstrated the feasibility of the optimized scenario.

| MARS LGA | NOMINAL SETUP | OPTIMIZED SETUP |
|---|---|---|
| NOMINAL $2B_L$ [HZ] | 25 | 152 |
| EQ. LOOP SNR [DB] | 3.18 | 11.35 |
| INFORMATION RATE [BPS] | 13.89 | 13.89 |
| $E_b/N_0$ [DB] | 21 | 21 |

Table 5-4: nominal and optimized scenarios setup (SEP = 1 deg).

In general, another area of optimization is the data rate. In fact, by trimming the data rate we can take the $E_b/N_0$ to the value requested by the coding scheme in presence of plasma. To this end, the baseband performance curves at different $FP$ values can be used to draw a data rate vs. $E_b/N_0$ plane, divided by the baseband curve in two regions (Figure 5-1). The red region indicates from underperformance with respect to the target CER to non-operability. Larger information rates amplify the effect of the amplitude scintillation since a fading of certain duration would cause the loss of a larger number of bits (as by fading period definition). In order to reach the target CER it is therefore necessary to increase the available $E_b/N_0$to progressively larger values. The white line connects the points where the $E_b/N_0$ is sufficient to reach a 1E−3 CER at the given information rate (and the consequent fading period). Given a certain information rate, moving right of the point marked by the white line (larger $E_b/N_0$) the CER will be even smaller than 1E−3, thus defining a safe or operability region (green region). The white dots mark the position of the nominal contingency case in the plane. For Mars LGA scenario, the nominal data rate allows to stay in the green region, so no reduction is needed. Actually, Figure 5-1 shows that the data rate can be optimized.

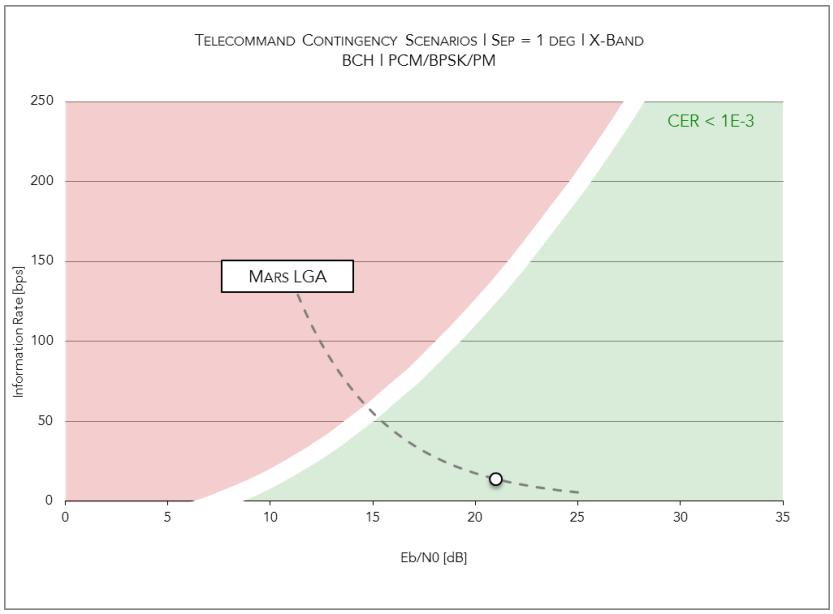


Figure 5-1: data rate vs $E_b/N_0$ plane, divided into operability (green) and non-operability (red) regions by the baseband curves.

## 6. PROPOSED TECHNICAL SOLUTIONS AND PERFORMANCE

The solutions proposed to mitigate the plasma scintillation cover the domains of coding techniques, modulation schemes and diversities techniques.

### 6.1. CODING TECHNIQUES

As there is a general and consolidated consensus about the adoption of the Low Density Parity Check (LDPC) codes for TC, namely the LDPC(128, 64) and the LDPC(512, 256) codes, as valuable alternatives to the current standard BCH code, such codes have been included in the list of possible solutions. The new short LDPC codes are described in detail in [AD 3]. As a further alternative, however, we have considered the opportunity to use short PCTCs to face the impact of solar scintillation over TC. As examples of non-standard codes for TC links, we have considered two PCTCs with rate $R_c$ = 1/2, information length $k$ = 64 bits and $k$ = 256 bits, in such a way as to have a perfectly fair comparison with the LDPC codes.

More precisely, in the following we have set, as an example, $FP$ = 8 encoded symbols for the simulations involving the LDPC codes. In order to have a (almost) fair comparison, that is fixing the same value of the bit rate but ensuring, at the same time, (almost) equal coherence times for the simulations, we impose that the value of $FP$ for the BCH(63, 56) code is 4 encoded symbols[2]. Table 6-1 shows the gain in dB of the LDPC and PCTC with respect to BCH. The short LDPC code has been decoded by using the hybrid algorithm while the long LDPC code uses the Normalized Min Sum (NMS) algorithm. The hybrid decoding algorithm may provide error rate performance significantly better than the NMS algorithm. Unfortunately, however, it cannot be applied to the long code for complexity reasons.

| | LDPC(128, 64) Hybrid algorithm | LDPC(512, 256) NMS algorithm | PCTC(128, 64) | PCTC(512, 256) |
|---|---|---|---|---|
| M = 0.2 | 5.33 | 4.94 | 4.49 | 5.82 |
| M = 0.5 | 14.27 | 14.09 | 13.12 | 15.00 |
| M = 0.9 | 27.77 | 27.94 | 25.40 | 28.77 |

Table 6-1: coding gain (in dB) of the LDPC codes, with respect to the BCH(63, 56) code , at CER = 1E–3, in the MRL scenario with $FP$ = 8 encoded symbols and $m$ = 0.2, 0.5 and 0.9.

Although the best error rate performance is given by the PCTC(512, 256), its adoption (as well as that of PCTCs, in general) should be discouraged for a number of reasons. In particular:

1. Short PCTCs are out of the standard, and it is realistic to think that they will not be included in the standard. In fact, we must remind that PCTCs have been already evaluated by the Agencies, over the AWGN channel in view of updating the standard, but at the end they have been discarded. The reason for having finally chosen the LDPC codes are manifold, but are summarized in [AD 4] where, with reference to the selected code rate and lengths, it is said that "LDPC codes are well suited to such a code rate and blocklength, and in contrast to turbo codes, LDPC codes probably provide a wider range of implementation options to trade performance against speed and complexity".
2. Even when preferable, the extra-gain offered by the PCTC(512, 256) is rather small, and it becomes smaller and smaller for decreasing values of the error rate. Such a behavior is due to the error floor phenomenon, that is rather evident for short PCTCs while it appears later for short LDPC codes. As a consequence, if smaller target error rates are considered (that is a realistic hypothesis for future, more and more demanding missions), it is highly probable that LDPC codes outperform the PCTCs also for those scenarios where presently the reverse occurs.

[2] Rigorously, the value of $FP$ for the BCH(63, 56) code should be a fraction 0.5625 of the $FP$ for the LDPC codes. So, for $FP_{\mathrm{LDPC}}$ = 8 encoded symbols it should be $FP_{\mathrm{BCH}}$ = 4.5 encoded symbols. The choice $FP_{\mathrm{BCH}}$ = 4 encoded symbols, instead of $FP_{\mathrm{BCH}}$ = 4.5 encoded symbols, corresponds to introduce the simplifying assumption of an integer number of encoded symbols affected by the same fading. Assuming, for example, $R_b$ = 1 kbps, this corresponds to have $T_c$ = 4 ms for the LDPC codes and $T_c$ = 3.56 ms for the BCH code, that is a rather small difference.

3. In the presence of solar scintillation, the LDPC codes become preferable for large coherence times and high scintillation indexes, that is for unfavorable propagation conditions. Since the aim of the use of coding should be to maintain a limited value for the transmitted power, it is better to have greater coding gains where the required SNR is large.

For TM as well, the proposed solution consists in LDPC codes, which have been already included in the TM Synchronization and Channel Coding recommendation [AD 5] with different lengths and rates. In particular, we can consider the LDPC(32768, 16384), the LDPC( 8192, 4096) and the LDPC(2048, 1024) codes.

Although having different length, the performance of these LDPC codes can be compared to that of PCTC(17848, 8920), having the same code rate. An example is shown in Table 6-2 for the case of *FP* = 150 encoded symbols. As usual, different values of *m* are considered. All the LDPC codes are decoded by using the NMS algorithm.

It is evident that the LDPC(32768, 16384) code is able to outperform the PCTC(17848, 8920) for any value of the scintillation index. The LDPC(8192, 4096) code is worse than the PCTC(17848, 8920) for *m* = 0.2 but its performance becomes better than that of the PCTC(17848, 8920) for *m* = 0.5 and *m* = 0.9. The LDPC(2048, 1024) code, instead, is always beaten by the PCTC(17848, 8920) but this was somehow expected because of its significantly smaller length.

| | LDPC (32768, 16384) | LDPC (8192, 4096) | LDPC (2048, 1024) | PCTC (17848, 8920) |
|---|---|---|---|---|
| *m = 0.2* | 1.15 | 1.60 | 2.65 | 1.50 |
| *m* = 0.5 | 2.19 | 3.40 | 6.00 | 5.48 |
| *m* = 0.9 | 5.58 | 8.32 | 13.90 | 13.47 |

Table 6-2: $E_b/N_0$ values (in dB) required to achieve CER = 1E−5 for the various considered codes in the MRL scenario with *FP* = 150 encoded symbols; amplitude scintillation only.

Table 6-3 reports a similar comparison for *FP* = 3500 encoded symbols.

| | LDPC (32768, 16384) | LDPC (8192, 4096) | PCTC (17848, 8920) |
|---|---|---|---|
| *m = 0.2* | 2.47 | 3.92 | 2.93 |
| *m* = 0.5 | 7.61 | 25.28 | 20.56 |
| *m* = 0.9 | 17.74 | 44.01 | 47.98 |

Table 6-3: $E_b/N_0$ values (in dB) required to achieve CER = 1E−5 for the various considered codes in the MRL scenario with *FP* = 3500 encoded symbols; amplitude scintillation only.

So, even more than for TC links, as discussed above, we can say that the adoption of LDPC codes provide a valid alternative to the PCTCs also for TM links. The main merits of LDPC codes is in the fact they are less sensitive to the impact of (relatively) slow fading (like that occurring in the MRL scenario, in particular), which instead is responsible for the appearance of a sort of "error floor" in the case of PCTCs. As mentioned, these codes are already included in the TM Synchronization and Channel Coding standard [AD 5], so that their use in future missions can be easily planned at no additional cost.

Possible inclusion of an interleaver to mitigate the impact of long fading periods has been also considered. It has been shown that significant gains can be achieved, with respect to the system without interleaver, on condition that the coherence time is not too long. When heavy fading influences several consecutive codewords, the designed interleaver is not effective and it is necessary resorting to different approaches.

Finally, an analysis on the inclusion of erasure correcting code has shown improved performance over both normal transmission and the adoption of a codeword interleaver. This is achieved at some costs in terms of latency and complexity. Using an interleaver is still a viable solution as long as the interleaver length is considerably longer than FP, and produces a limited loss in performance with respect to the use of an ideal erasure correcting code of the same dimension. On the contrary, for large values of FP, the solution based on relatively short interleavers does not provide significant advantages over normal transmission, while resorting to an erasure correcting code still allows to achieve significant performance improvements over normal transmission. In short, erasure codes are not so difficult to decode, but they are not yet foreseen for imminent standardization.

### 6.2. MODULATION SCHEMES

While the use of different coding schemes can improve the performance of the link for standard modulations, the use of different modulation schemes is justified only when coherent demodulation cannot be used. In fact, there might be contingency cases in which the power limited conditions and the low SEP angle result in impairment of carrier tracking in the PLL. In such cases, non-coherently demodulated schemes, such as *M*-FSK, can be used, thus avoiding the adoption of a PLL that is sensitively affected by the scintillation noise. In fact, a coherent detection of *M*-FSK, carried out by means of phase reconstruction and separated matched filters, is possible, but it would lead to a 3 dB loss with respect to PCM/BPSK/PM. The actual advantage of using non-coherent demodulation of FSK, that is about 1 dB worse than coherent detection, is its use in case of scintillation noise, where coherent demodulation would simply not work (if coherent demodulation was possible, that it would make sense to use PCM/BPSK/PM). Coherent modulations such as PCM/BPSK/PM are available on-board for moderate fading scenario or for nominal condition (actual modulation scheme would be selected by a dedicated command). So in principle we may have two receiver's configurations, selectable on-board, to be used according to the actual mission scenario. The same approach may apply to the Ground Station.

A first evaluation has been done for FSK and DPSK. The performance of the DPSK mo/demodulation scheme, though being significantly distant from that of the PCM/BPSK/PM scheme, is never worse than that of the 2-FSK scheme. On the other hand, contrary to PSK and DPSK, FSK modulation allows improving the error rate performance by increasing the cardinality of the constellation, that is, assuming $M > 2$ orthogonal waveform. So, a gain of about 3 dB are reached by the uncoded system, over the AWGN channel, for the error rates of interest, when passing from $M = 2$ to $M = 4$, practically compensating, over the AWGN channel, the gap with respect to DPSK. Even more, the error rate performance of uncoded 8-FSK with non-coherent demodulation becomes better than that of uncoded BPSK at $E_b/N_0 \approx$ 8 dB where the bit error rate is about 2E−4. The price to pay is in terms of enlarged bandwidth occupation, which in fact increases according to the classical law $M/\log_2 M$.

As in the present project the bandwidth has not been set as a constraint, we are justified to propose the adoption of *M*-FSK. A good candidate in this sense, for the reasons explained above, seems to be 8-FSK. Table 6-4 summarizes the values of $E_b/N_0$ required to have CER = 1E−3 for the LDPC(128, 64) code with Hybrid and NSM algorithms, using PCM/BPSK/PM and 8-FSK.

| | BPSK Hybrid | BPSK NMS | 8-FSK Hybrid | 8-FSK NMS |
|---|---|---|---|---|
| CER = 1E-3 | 7.54 | 10.75 | 11.18 | 14.43 |

Table 6-4: $E_b/N_0$ values (in dB) required to achieve CER = 1E−3 and CER = 1E−5 for PCM/BPSK/PM modulation and different LDPC(128, 64) decoding schemes.

The results obtained confirm that the error rate performance of coded non-coherent *M*-FSK schemes is worse than that of the coded coherent (PCM/BPSK/PM) scheme (we have verified the same conclusion holds for $M = 16$). This is due to the fact that consolidated decoding algorithms are optimized for coherent modulations and do not work equally well in the non-coherent case. On the other hand, to develop decoding algorithms which are more suited for non-coherent schemes (FSK in particular) is an open (not simple) issue and, to the best of our knowledge, no proved strong method is available, for such a purpose, in the literature.

#### 6.2.1.1. MERCURY LGA WITH 8-FSK NON COHERENT DEMODULATION

The actual usefulness of 8-FSK can be seen in contingency scenarios in which the tracking of the carrier with a PLL is simply not possible, due to the too low equivalent loop SNR. This is the case for an examined generic scenario to Mercury with an LGA, in which the equivalent loop SNR attainable affects dramatically a PLL on a residual carrier. This results in the impossibility to establish a reliable link with a PCM/BPSK/PM modulation scheme.

Non-coherent demodulation of an 8-FSK signal has been therefore analyzed in order to overcome the phase scintillation effect. End-to-end tests results are shown in Table 6-5. The case is successful even with BCH(63, 56), but can be further optimized with LDPC codes, which have been implemented in the end-to-end software with 8-FSK. In this case, the gain is provided by the intrinsic performance of LDPC with respect to BCH, and not by the use of *M*-FSK. In fact, as previously stated, the decoding algorithms are optimized for coherent modulations.

The 8-FSK modulation scheme permits to establish a reliable link, overcoming the phase scintillation issue, which is disruptive for coherent demodulation approaches.

| 8-FSK<br>MERCURY LGA | LDPC(128,64)<br>HYBRID |
|---|---|
| $E_B/N_0$ [DB] | 8.0 |
| INFORMATION RATE [BPS] (INCREMENT) | 100.00 (+1340%) WITH RESPECT TO NOMINAL VALUE (BCH) |
| TEST RESULTS | OK |

Table 6-5: End-to-end 8-FSK test results for Mercury LGA scenario (SEP = 1 deg).

### 6.3. SYSTEM SOLUTIONS

The system solutions are conceived to minimize the impact on the on-board transponder. The concept of diversity is the combination of signals that, under certain circumstances, undergo different fading. In the space diversity, the same signal is received at two (or more) stations. Depending on the distance between the stations, the signal may undergo a different fading, and the combination of the signals can lead to an overall improvement. The optimum distance between the stations can be determined via independent simulations.

The frequency diversity, on the other hand, is another system solution that can be used to improve the link performance without changing the property of the link, such as modulation scheme and coding technique. It consists in having two signals at different frequencies, and combining them to recover bits that would be lost with one signal only. In this case the redundancy is on the channels; basically, two carriers on different channels, if separated appropriately in frequency, undergo different fading amplitude, and their combination provides an improvement with respect to one channel only.

#### 6.3.1. SPACE DIVERSITY

An independent simulation with the thin screen approximation, valid for downlink, has been conducted to assess the minimum distance between two Ground Stations to verify the assumption that the plasma is uncorrelated. Figure 6-1 shows the probability that the fading amplitude in a given range is simultaneously present at two Ground Stations as a function of their distance.

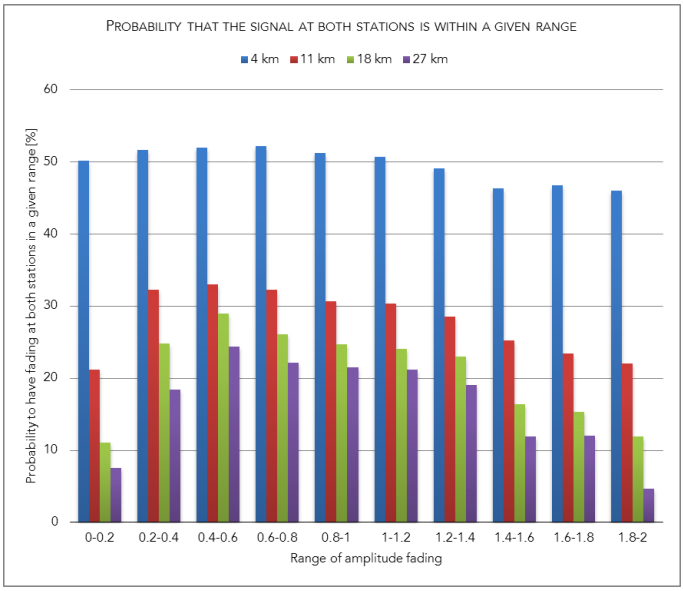


Figure 6-1: probability that the amplitude fading assumes a value within a given range at both stations as a function of the distance between two points on the screen.

According to Figure 6-1, the probability to have the amplitude fading at both stations between 0 and 0.2 is about 7% for a distance of 27 km. It has to be noted that, for a given distance, the sum of the probability values is not 1 because the basis for the calculation of the probability is always different

### 6.3.2. FREQUENCY DIVERSITY

The limit of the frequency diversity approach is in terms of intermodulation products, when more than one carrier is transmitted. The behavior of a microwave High-Power Amplifier (HPA) can be represented by means a non-linear and memory-less model that exhibits non-linear gain (AM/AM characteristic) and amplitude-to-phase conversion (AM/PM characteristic). This kind of modelling allows estimating the intermodulation products of a non-linearity operating on multi-carrier inputs, such as the considered Ka-Band Travelling Wave Tube Amplifier (TWTA).

Simulations with two carriers, separated by 200 kHz, with a subcarrier of 16 kHz and telemetry modulation index of 1 rad-pk have been carried out. The measured AM/AM and AM/PM curves reported in Figure 6-2 have been used as well representative of typical TWTAs' non-linearity.

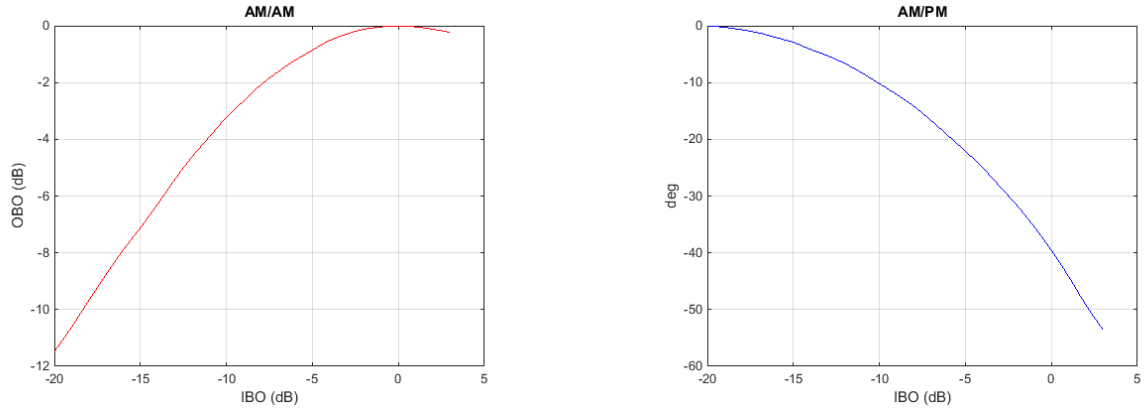


Figure 6-2: typical AM/Am and AM/PM curve for on-board TWTA (measured).

Simulation results in terms of downlink RF spectrum at the TWTA output are reported for several values of IBO.

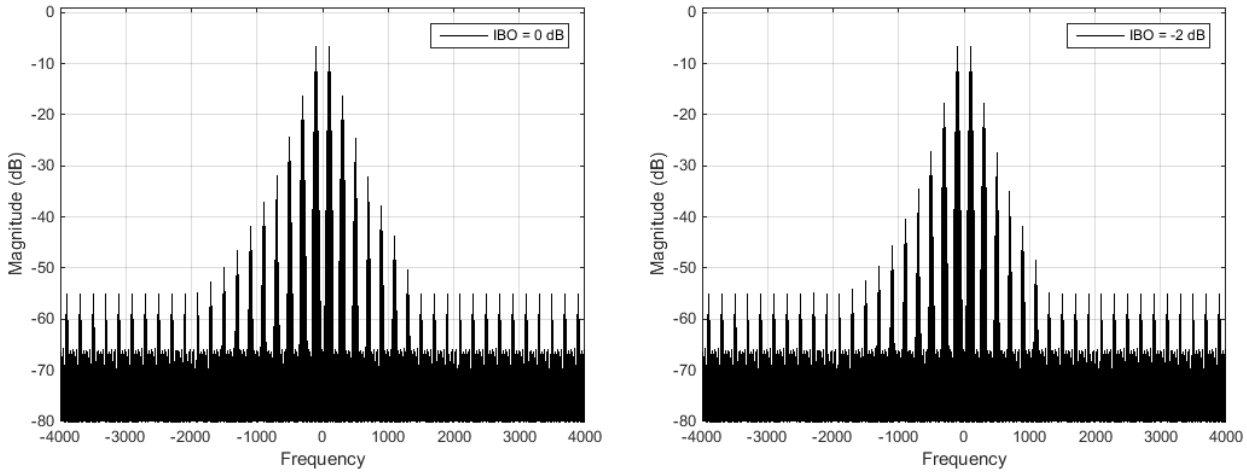


Figure 6-3: level of intermodulation products for IBO = 0 dBm (left) and IBO = –2 dBm (right) (frequencies in kHz).

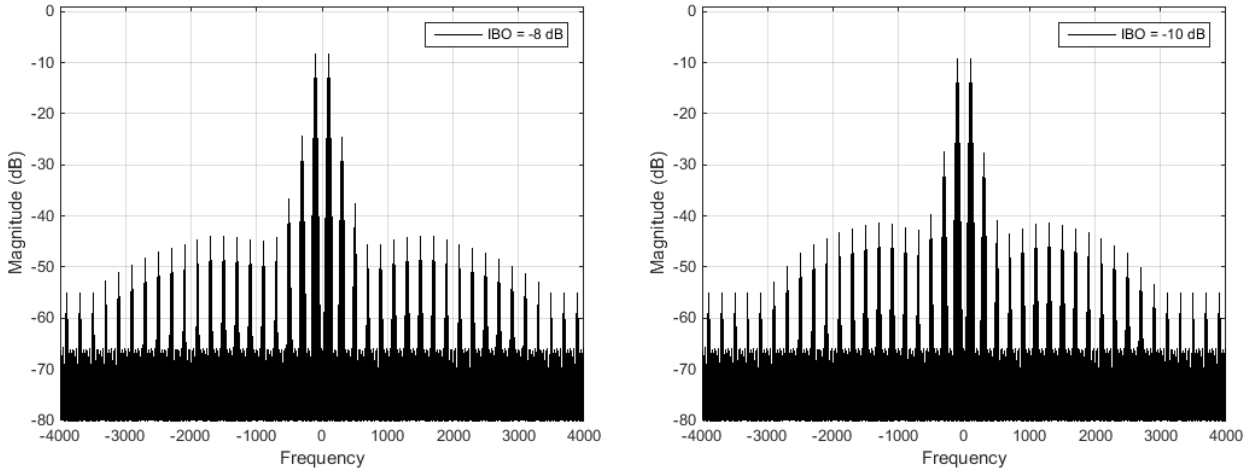


Figure 6-4: level of intermodulation products for IBO = –8 dBm (left) and IBO = –10 dBm (right) (frequencies in kHz).

## 6.4. SUMMARY

### 6.4.1. CODING

First of all, coding technique area has been further investigated. Short turbo codes (telecommand) performances have been assessed by means of baseband simulations. Results show that the hybrid implementation of LDPC(128, 64) code outperforms the PCTC(128, 64) code in any considered operation scenario, while, at CER = 1E−3, PCTC(512, 256) is slightly better than the LDPC(512, 256) code, in almost all conditions. Even if PCTC(512, 256) seems to be preferable in most of the considered conditions, several issues should discourage its adoption: first of all short PCTCs are out of the present day standard, and it is realistic to think that they will be not included, in reasonable times, in the standard. Moreover, the extra-gain offered by the PCTC(512, 256) is rather small and it is destined to decrease for lower values of error rate, because of the early appearance of a floor. Additionally, in the presence of solar scintillation, the LDPC codes become preferable for large coherence times and high scintillation indexes, that is for unfavorable propagation conditions.

Regarding TM links, focusing attention on the code rate $R_c$ = 1/2, the performance of the PCTC(17848, 8920) has been compared with that of the standard LDPC codes with the same code rate and different lengths. Baseband simulations have shown that: i) except for high error rates, the LDPC(32768, 16384) code is able to outperform the PCTC(17848, 8920) for any value of the scintillation index *m*; ii) the LDPC(8192, 4096) code is worse than the PCTC(17848, 8920) for $m$ = 0.2 but its performance becomes better than that of the PCTC(17848, 8920) for $m$ = 0.5 and $m$ = 0.9; iii) The LDPC(2048, 1024) code is always beaten by the PCTC(17848, 8920). Similarly, for $FP$ = 3500 encoded symbols, baseband simulations have shown that: i) the LDPC (32768, 16384) code outperforms the PCTC(17848, 8920) for any considered value of *m*; ii) the LDPC(8192, 4096) code has better performance than that of the PCTC(17848, 8920) only for $m$ = 0.9. In both the considered cases, the signal-to-noise ratio required by the LDPC(32768, 16384) code is significantly smaller than those required by the other codes, although this is paid with a larger, although still affordable, complexity. The rationale of this behavior (and, more generally, the reason of the better performance than TM LDPC codes show w.r.t. codes), can be found in their greater robustness to the appearance of error floor phenomena. As the presence of amplitude scintillation obliges to work at very high signal-to-noise ratios, where the error floor becomes evident, this favorable behavior of the LDPC codes provides a significant advantage.

### 6.4.2. MODULATION

From the modulation perspective, baseband simulations have shown that, when coherent detection is possible, (equivalent loop SNR allows tracking of the phase) the PCM/BPSK/PM modulation offers better performances. In fact, the lower efficiency of non-coherent modulation schemes in exploiting error correcting codes (on the basis of the consolidated decoding algorithms) does not permit 8-FSK to overcome PCM/BPSK/PM for error rates of practical interest. When the tracking of the phase is not possible, non-coherent demodulation of FSK offers the possibility to have a successful link, even if not particularly performant in terms of achievable information rate.

### 6.4.3. DIVERSITY

Two system diversity approaches have been studied. In the first one, two antennas have been considered to receive the same signal, and, under the assumption that the signal at each station undergoes different plasma scintillation, this would allow, through a combination process on-ground (this approach is valid only for downlink), to recover data that would be lost with one station only. A numerical assessment using the thin screen approximation has been conducted to define the minimum distance by which two stations should be separated to have de-correlated plasma. Interesting results at 1 deg are reported: in particular, the probability of detecting a severe fading amplitude at both stations decrease dramatically (below 10%) when the stations are separated by 27 km. A probability tending to zero means that the signal can be recovered as if it were not affected by plasma.

Finally, a simulation on frequency diversity has been carried out. The frequency diversity is the transmission of two carriers simultaneously. Such signals, provided that their separation in frequency is larger than the coherence bandwidth, undergo different plasma scintillation. The simulation was aimed at computing the out-of-band emissions in case of transmission of two carriers for different values of the IBO.

# 7. IMPLEMENTATION OF TECHNICAL SOLUTIONS AND ROADMAP

Support of additional functions, like new modulation formats for both telecommand and telemetry, up-link LDPC decoding, requires the use of a dedicated space-qualified Field Programmable Gate Array (FPGA) that will support the Application Specific Integrated Circuit (ASIC) for the additional required processing tasks. The choices are the RTAX family (antifuse FPGA) and the RTG4 family (flash-based).

## 7.1. IMPLEMENTATION OF LDPC DECODING

With reference to low-density parity-check codes with $k = 64$, $n = 128$ and with $k = 256$, $n = 512$, these codes can be accommodated on-board through the FPGA. These codes are in fact close to be included in the Consultative Committee for Space Data Systems (CCSDS) standard for Telecommands[3]. The reference decoding algorithm (that is not specified by the standard) is the NMS, which is an iterative algorithm.

The following hypotheses apply:

- FPGA selection among already available devices fulfilling space requirements; in particular, due to TAS-I heritage, RTAX and RTG4 FPGAs have been considered, both provided by Microsemi.
- Not too high bit rate; a maximum value will be given in the following, which will be however compatible with telecommands needed also for Near-Earth missions.
- Decoding latency less than telecommands duration.
- Soft decisions coming from demodulator are assumed to be represented with less than 6 bits.
- Processing clock frequency: 100 MHz.

Furthermore, for the complexity analysis we have focused on the (512, 256) code. The description below is very short and compact. Details can be found in the literature.

The LDPC decoder is completely described by the by-parted Tanner Graph, partially shown in Figure 7-1 for the (128, 64) code (only outgoing connections of first so-called v-nodes and first so-called c-nodes are shown).

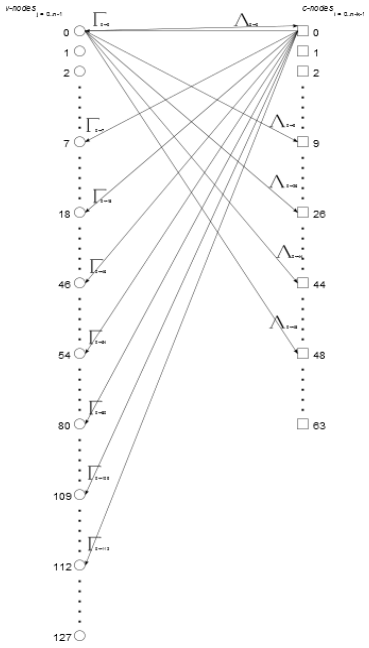


Figure 7-1: Tanner graph.

[3] The implementation of LDPC decoder in on-ground receivers is less critical [RD 4]. The new ESA receiver TTCP already accommodates the decoding LDCP codes of interest for telemetry.

LDPC processor is in charge of Λ and Γ messages elaboration, to be sent to v-nodes and c-nodes respectively. If we look at the **H** matrix (the parity-check matrix), we can see that for each c-node we have always 8 messages from v-nodes, (for both codes), and for each v-node the number of messages from c-nodes ranges from 3 to 5. So, the number of messages to be generated will be (at most) 5×512 for the v-nodes and 8×256 for the c-nodes.

Coming to the computational complexity required for each type of message, we can say that for the Λ messages the following operations are required:

- Selection of minimum absolute value among the incoming eight: this is evaluated 8 times discarding in turn one of the inputs. This operation requires 7×8 binary comparators with $q$ ($q$ = 6, in particular) bits, and 8 $q$-bits multiplexers. A Rough Order of Magnitude (ROM) estimate of the related combinatorial logic is about 720 LUTs.
- Signs product: 8 7-inputs XOR, equivalent to about 56 LUTs.
- Results normalization: 8 multipliers 6×8 bits (we assume the 0.8 fixed coefficient to be represented with 8 bits, with an error less than 0.1%). This requires 60×8 = 480 LUTs.
- Registers for the input/output messages: 8×6×2 = 96 FF

Conversely, the Γ messages elaboration will require:

- 5 (max) 6-bits adder: about 30 LUTs
- Results normalization : 5 multipliers 6×8 for about 300 LUTs
- Input/Output registers : 5×6×2 = 60 FF

Furthermore, two Dual-Ported Random Access Memories (DPRAMs) are required, to store all messages, as well as an input buffer for the input codeword (6×512 FF). The two DPRAMs should be replicated by 2 to allow a ping-pong access, and their dimensions should be 5×512×6 and 8×256×6 bits respectively. The total amount of Random Access Memory (RAM) needed should be 55296 bits.

Please note that in this estimate only the main processing elements are taken into account: Control and addressing logic is not considered, neither the iteration control logic.

With these numbers at the hand, it is evident that a completely parallel solution, with 256 Λ processors and 512 Γ processors working together, would not fit in the selected FPGAs, even considering only the LUT needed. In fact, it would require (1176×256 + 330×512) = 470K LUTs, while the RT4G150 device has about 150K LUTs and the RTAX4000S about 37K LUTs. A partially parallel solution is therefore envisaged, with just one Λ processor and one Γ able to process at one time all messages coming in the node. Total complexity should be therefore:

| LUT | Flip-flop | RAM bits |
|---|---|---|
| 1586 | 172 | 55296 |

While the time required at every iteration should be:

- For Λ messages: 8$T$ ($T$ being 1 ns) to read messages from v-nodes, 2$T$ to compute, 8$T$ to write them back. This will be repeated 256 times, so 18×256×$T$ = 46 μs
- For Γ messages: 5$T$ to read messages from c-nodes, 2$T$ to compute, 5$T$ to write them back. This will be repeated 512 times, so 12×512×$T$ = 61.4 μs

Every iteration should last about 107 μs. A decoding loop of 20 iterations should last 2.1 ms.

Maximum bit-rate allowed may be estimated as 512/2.1 ms = 243 kbit/s. Some kind of access optimization may be found, to arrange messages storage in order to reduce access time: this should be exploited to increase the bit-rate and/or to the number of iterations.

In addition, for Deep Space missions featuring low symbol rates (i.e. up to a few hundreds of bit per seconds), the LEON2 Microprocessor may be used to support the Most Reliable Basis (MRB) algorithm in the Hybrid Decoder configuration while the iterative decoding will be in charge of the FPGA. The hybrid decoder principle is shown in Figure 7-2.

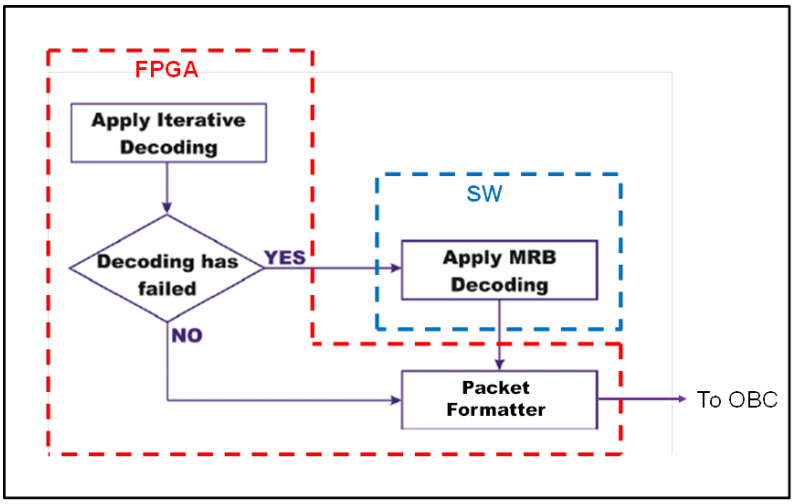


Figure 7-2: hybrid decoder implementation.

In order not to modify the current interface between the TT&C Transponder and the On-board Computer (OBC), the decoder output shall be properly formatted building-up the TC packet composed of Communications Link Transmission Unit (CLTU and the Coding Layer.

## 7.2. IMPLEMENTATION OF 8-FSK

The 8-FSK modulation format may be supported with the existing X-Deep Space Transponder (X-DST) product platform properly customizing the BB-FPGA and the relevant digital Printed Circuit Board (PCB). A top-level block diagram of such equipment is provided in Figure 7-3.

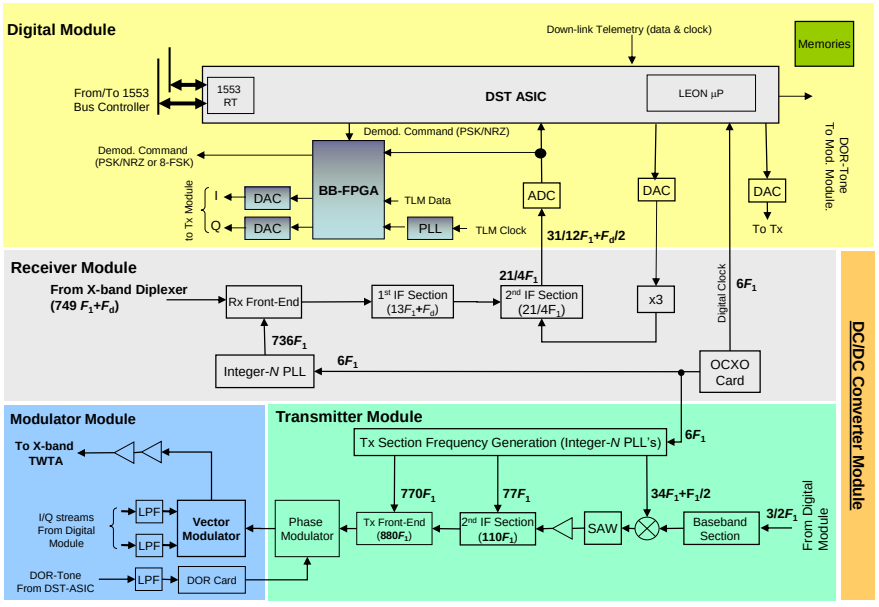


Figure 7-3: X-DST top-level block diagram including 8-FSK capabilities.

In addition to the legacy functions, the BB-FPGA shall include the building blocks here below:

- A Direct Digital Synthesizer in charge of synthesizing the down-link FSK tones. For each 8-FSK symbol, the Direct Digital Synthesizer will generate the in-phase and quadrature frequency that will be converted in the analogue domain, low-pass filtered and then routed to the X-Band Vector Modulator operating as a Single Side-Band (SSB) modulator.
- A non-coherent 8-FSK receiver operating on the digitized Intermediate Frequency (IF) sample and supported by the relevant synchronization algorithms at carrier and symbol-level.
- An output multiplexer in charge of forwarding to the OBC the demodulated commands that are provided by the DST ASIC in case of standard PM/BPSK/NRZ signaling or directly by the BB-FPGA in case of 8-FSK (i.e. under severe scintillation).

### 7.3. FREQUENCY AND SPACE DIVERSITY

From the on-board perspective, two down-link Direct Digital Synthesizers can be used for dual-band down-link applications. This is a feature already present on BepiColombo Ka band transponder (KaT). The transmission scheme is represented in Figure 7-4. The frequency spacing between $f_1$ and $f_2$ could be 8-10 MHz (within the Surface Acoustic Wave (SAW) filter bandwidth). The scheme can be implemented on the available H/W, limiting the cost and the level of criticality.

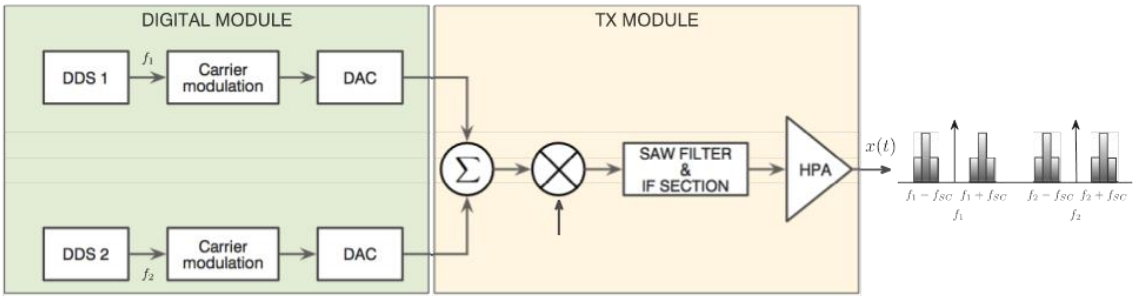


Figure 7-4: transmission scheme implemented on BepiColombo KaT.

On ground, the two signals can be open loop registered in different channels of the receiver, centered at different frequencies. Ideally, to exploit the full advantage of having two signals, the signals could be combined before the demodulation. This way, there is an increase of the loop SNR in the PLL, which would act directly on the combined signal, allowing for a smaller degradation. In this technique, called Full Spectrum Combining, the differential delay and phase must be estimated between the two stations. Such estimate requires a cross-correlation between the two data streams. In this specific case, the rapid change of the phase due to scintillation and the continuously changing amplitude of the signal would make the cross-correlation, and the consequent estimate of differential phase, very difficult, if not unfeasible, especially for low SEP angles.

The solution is to use a different combination method, called Symbol Stream Combining, where the two signals are separately demodulated and then combined before the decoding process. In this process, we have to assume that the PLL is able to track the signal, that is the equivalent loop SNR is above the feasibility threshold (7 dB). The demodulation approach is shown in Figure 7-5.

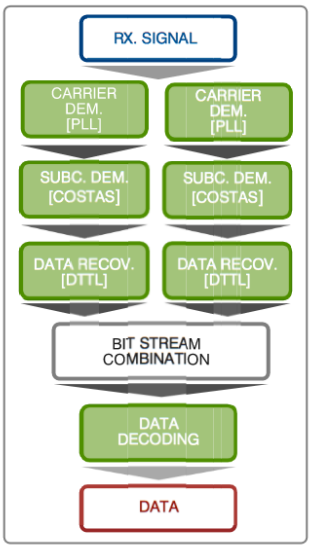


Figure 7-5: demodulation approach for Symbol Stream Combining.

Regarding the space diversity, there are no changes on-board the spacecraft. The requirements on-ground are the availability of another station and the presence of a tool performing the Symbol Stream Combining combination process, exactly the same as of the frequency diversity (Figure 7-5).

### 7.4. ROADMAP

A roadmap for the proposed solutions – LDPC decoding, non-coherent demodulations, frequency diversity and space diversity – is presented in Table 7-1. The timeline for the implementation of the solutions, involving modifications to the transponder and S/W tools to be used on-ground for frequency and space diversity, together with TRL mapping and costs, is also reported. All the solutions are technically implementable in a timeframe of two years. LDPC decoding and non-coherent demodulations require modifications to the transponder, after the validation of the prototypes, and consequently cannot be accommodated on-board flying or next-to-flight missions whose design is already frozen. Space diversity, instead, relies on a S/W tool to be used on-ground, and this makes the solution viable for all the missions.

| Item/Function | Outline of implementation | Implementation steps | Timeline | ROM costs | Non-recurring ROM cost for the 1st program | Applicability to flying or next-to-flight missions |
|---|---|---|---|---|---|---|
| **LDPC Decoding on-board**.<br>The LDPC decoder for TC is implemented as per Section 7.1 following output from previous ESA study "*Next Generation Uplink Coding Techniques*" (NEXCODE). | An LDPC decoder breadboard developed by DEIMOS will be validated together with DST Engineering Model in the frame of the on-going ESA study "Flexible and Autonomous TT&C Transponders for Multi Mission Applications" (FAT). Then the relevant VHDL IP has to be synthesized towards space-qualified FPGA (baseline: RTG4). | Breadboard validation – TRL 3<br>Synthesis towards RTG4<br>Validation at DST-level using RTG4 prototype – TRL 5 | 4Q/2017<br>T0+2m<br>T0+6m | COVERED BY FAT<br>150 K€ | 70 k€. It includes electrical redesign of the Digital, updating of the manufacturing documentation and delta-analysis (WCA, PSA, etc).<br>DEIMOS cost for LDPC IP to be assessed. | NO |
| **M-FSK TC Demodulator on-board.**<br>The DST supports 8-FSK or 16-FSK in addition to the standard telecommand modulation formats. The operative signalling scheme has to be selected by a dedicated | A space-qualified FPGA (baseline: RTG4) will integrate the relevant signal processing blocks. Such FPGA may also include down-link GMSK/*M*-FSK/ processing. | Algorithm definition<br>Specification<br>VHDL Design & Simulation<br>Breadboard test – TRL 3<br>Validation at DST-level – | T0+2m<br>T0+4m<br>T0+8m<br>T0+12m | 350 K€ | 80 k€. It includes electrical redesign of the Digital, updating of the manufacturing documentation and delta-analysis (WCA, PSA, etc). | NO |

| | | | | | | |
|---|---|---|---|---|---|---|
| 1553 command. | | TRL 5 | T0+15m | | | |
| | | Specification | T0+4m | | | |
| | | VHDL Design & Simulation | T0+8m | | | |
| | | Breadboard test – TRL 3 | T0+12m | | | |
| | | Validation at DST-level – TRL 5 | T0+15m | | | |
| **M-FSK TM Modulator on-board.**<br>The DST supports *M*-FSK in addition to other telemetry modulation formats (residual carriers and suppressed carrier). The operative signalling scheme has to be selected by a dedicated 1553 command. | A space-qualified FPGA (baseline: RTG4) will integrate the relevant signal processing blocks proving to the X-Band Vector Modulator the in-phase and quadrature modulating streams according to the selected modulation format. Such FPGA may also include *M*-FSK or, alternatively, TC Demodulator. | Algorithm definition | T0+1m | 200 K€ | 80 k€. It includes electrical redesign of the Digital, updating of the manufacturing documentation and delta-analysis (WCA, PSA, etc). | NO |
| | | Specification | T0+3m | | | |
| | | VHDL Design & Simulation | T0+6m | | | |
| | | Breadboard test – TRL 3 | T0+9m | | | |
| | | Validation at DST-level – TRL 5 | T0+12m | | | |
| **Frequency diversity**<br>The same signal in PM/BPSK/NRZ or PM/SP-L modulation format is transmitted in X-Band with a frequency separation in the range from 8 to 10 MHz. | It requires a modification of the X-Band Transmitter module in the relevant Baseband section that needs to combine the two down-link signals at the input of the frequency conversion stages. | The hardware modification is straightforward and does not require a specific validation phase through breadboard. It can be directly pursued in the frame of a flight Program. | N/A | N/A | 60 k€. It includes electrical redesign of the X-Band Transmitter Module, updating of the manufacturing documentation and delta-analysis (WCA, PSA, etc). | YES. JUICE TRANSPONDER, FOR INSTANCE, IS A X/X/KA UNIT EQUIPPED WITH MULTIPLE DDS. |

| | | | | | | |
|---|---|---|---|---|---|---|
| A tool is used on-ground to combine the signals after demodulation. | The tool is an output of the study "Prototype of Off-line Correlator for Arraying Of Large Aperture Antennas" (PROTOCOL). | Breadboard Validation | 1Q/2018 | N/A | Covered by study "Prototype of Off-line Correlator for Arraying Of Large Aperture Antennas". | |
| | | Validation for operations (extensive test campaign) | T0+12m | N/A | 150 K€ | |
| **Space diversity**<br>The signal is acquired at two Ground Stations. A tool is used on-ground to combine the signals after demodulation (same tool as for frequency diversity). | The tool is an output of the study "Prototype of Off-line Correlator for Arraying Of Large Aperture Antennas" (PROTOCOL). | Breadboard Validation | 1Q/2018 | N/A | COVERED BY STUDY PROTOCOL | YES |
| | | Validation for operations | T0+12m | N/A | 200 K€ | |

Table 7-1: timeline and costs for the proposed solutions.

The new ESA receiver, TTCP, already accommodates the decoding of LDPC(32768, 16384), LDPC(8192, 4096) and LDPC(2048, 1024) [AD 6]. TTCP accommodates also the LDPC codes with rate 2/3 and 4/5, that have been also subject of the study. The algorithms for *M*-FSK modulation and demodulation can be applied also on-ground, with significant reduction of costs with respect to the on-board counterpart.

## 8. CONCLUSIONS

The RESCUe study has deeply investigated how a TT&C system for deep space missions can be improved to mitigate the plasma scintillation during superior solar conjunctions. The study aimed at defining technical solutions, together with a timeline for the next 10 years, to be adopted for flying, next-to-flight and future missions.

In order to build a robust mathematical model to be used for numerical simulations, data from Mars Express in 2013-2015 and Cassini in 2001-2002, acquired during superior solar conjunctions, have been used to validate the fading channel properties available in literature, on one hand, and to describe the characteristics of amplitude and phase scintillation, on the other hand. A S/W end-to-end simulator has been implemented, capable of reproducing the synchronization loops of the receiver. A baseband tool has been also used, under ideal circumstances, to characterize the performance of a large variety of coding schemes.

The first, important, result of the study is a full characterization of the behavior of the PLL with an incoming signal affected by plasma scintillation. The phase scintillation generates a loop phase error variance inversely proportional to the loop bandwidth, whereas the thermal noise in the loop is proportional to the bandwidth. This results in a *U*-shape of the loop error variance as a function of the $P_c/N_0$, allowing to derive an analytical expression for the optimum bandwidth. The expression for the equivalent loop SNR has been derived too, allowing to define a range of operability for the PLL (threshold for the equivalent loop SNR is 7 dB).

The definition of a range of operability for the PLL bandwidth has been a crucial point of the study. In fact, it allowed to carry out numerical simulations in two different conditions. In the first one, the PLL bandwidth is assumed to be such that the equivalent loop SNR is well above the threshold, so that baseband simulations can be performed assuming there are no synchronization error (this condition usually occurs where the $P_c/N_0$ is large, so that a large bandwidth can be tolerated also from a thermal point of view). In the second condition, we have evaluated contingency scenarios, in which the power and SEP conditions are such that the synchronization errors cannot be ignored (and sometimes the PLL cannot lock on to the signal); in this scenario the end-to-end software was used. Clearly, the end-to-end simulator shows the same results of the baseband tool in ideal conditions.
The results of the simulations indicate that:

- The approach currently followed during solar superior conjunction to determine the real $P_c/N_0$ shall not be based simply on adding a loss to the available power to noise density ratio, but rather shall consider the plasma effects in the choice of the PLL bandwidth, and consequently in the equivalent loop SNR. The simulations with ENTRuST have demonstrated that for power-limited conditions, which represent extreme scenarios, the re-definition of the PLL bandwidth can lead to a successful case;

- LDPC codes resulted to be more efficient than currently used coding schemes to mitigate the plasma scintillation. This has been demonstrated with baseband simulations and end-to-end tests, which have confirmed how also the contingency cases can benefit from the adoption of LDPC codes. The choice is also influenced by the fact that LDPC codes are already present in the TM standard and are close to be included in the TC standard.

- With current coding techniques, but also with the proposed LDPC codes, the non-coherent demodulated schemes can be beneficial for the plasma scintillation. It must be recalled that the performance of non-coherent demodulated schemes, such as *M*-FSK, is certainly poorer than coherent modulation of PCM/BPSK/PM. In this regard, when coherent modulation is possible (provided that the equivalent loop SNR is above the threshold) it does not make sense to use *M*-FSK, which would give worse performance. Rather, when the signal cannot be coherently demodulated, *M*-FSK can be a valuable alternative, at the cost of a lower data rate.

- Finally, system solutions, such as space and frequency diversity, have been assessed. Although space diversity offers a large gain that frequency diversity, it requires the availability of two Ground Stations. On the other hand, frequency diversity requires modifications on the transponder, but it is straightforward and does not require a validation phase through breadboard; it does not require two Ground Stations, but poses a limitation on the IBO level to limit the intermodulation products.

The implementation of LDPC decoding and non-coherent demodulated schemes require the implementation of a breadboard (TRL 3) and a phase validation at DST level (TRL 5), but the steps can be carried out in a couple of years. Of course, such solutions cannot be used on flying or next-to-flight missions, but only on future ones. Table 8-1 summarizes what currently available and proposed solutions for modulation and coding.

On the other hand, space and frequency diversity are solutions that can be applied also in the frame of current or next-to-flight missions. Data can be acquired at the Ground Station and post-processed offline, also in absence of an integrated S/W tool.

| Currently available | Proposed solution | Implementation steps | Applicability next-to-flight missions |
|---|---|---|---|
| BCH for TC. | LDPC(128, 64)<br>LDPC(512, 256)<br>Hybrid algorithm | • Breadboard validation – TRL 3<br>• Synthesis towards RTG4<br>• Validation at DST-level using RTG4 prototype – TRL 5 | NO |
| RS+CC for TM<br>PCTC(17848, 8920) for TM<br>PCTC(35696, 8920) for TM<br>PCTC(53544, 8920) for TM | LDPC(32768, 16384)<br>LDPC(8192, 4096)<br>LDPC(2048, 1024) | • Breadboard validation – TRL 3<br>• Synthesis towards RTG4<br>• Validation at DST-level using RTG4 prototype – TRL 5 | NO |
| PCM/BPSK/PM<br>PCM/SP-L | *M*-FSK TM Modulator and Demodulator. | • Algorithm definition<br>• Specification<br>• VHDL Design & Simulation<br>• Breadboard test – TRL 3<br>• Validation at DST-level – TRL 5 | NO |

Table 8-1: summary of what currently available and associated proposed solutions for modulation and coding